Supporting Information for:
Hollow nickel ferrite nanofibers templated using waste expanded polystyrene as electrocatalysts of the hydrogen evolution reaction

Rabiya J. Awan,[a,b] Zeliha Ertekin,[a] Senem Çitoğlu,[c] Hatice Duran,[c,d] Salman N. Arshad[b] and Mark D. Symes*[a]*

[a]*School of Chemistry, University of Glasgow, Glasgow, G12 8QQ, United Kingdom*

[b] *Department of Chemistry and Chemical Engineering, Syed Babar Ali School of Science and Engineering, Lahore University of Management Sciences, Lahore 54792, Pakistan*

[c] *Department of Materials Science & Nanotechnology Engineering, TOBB University of Economics and Technology, Söğütözü Cad. 43, Ankara, 06560 Türkiye*

[d] *UNAM — National Nanotechnology Research Center and Institute of Materials Science and Nanotechnology, Bilkent University, Ankara, 06800 Türkiye*

Materials and chemicals

Materials were obtained as follows: polyacrylonitrile with molecular weight 150,000 (25014-41-9; Sigma Aldrich), dimethylformamide 99.8% (68-12-2, Sigma Aldrich), nickel chloride hexahydrate 98% (7791-20-0; Lancaster Synthesis), iron chloride 98% (10025-77-1, Thermo Scientific), urea 98+% (52-13-6; Thermo Scientific), ammonium fluoride 98+% (121250-01-8; Thermo Scientific), absolute ethanol 99% (64-17-5; Fisher Scientific), Nafion solution (31175-20-9; Sigma Aldrich). All deionized water had a resistivity of 15 MΩ-cm. Expanded polystyrene was sourced from chemical packaging waste from the University of Glasgow's chemistry stores and was used without any further cleaning procedures. The elemental composition of the expanded polystyrene was confirmed by elemental analysis (Exeter CE-440), revealing a composition of C: 90% and H: 7.4%. Waste expanded polystyrene was dissolved in 500 μL of $CDCl_3$ (99.8% D, Cambridge Isotope Laboratories, Inc.) and analysed by nuclear magnetic resonance (NMR) spectroscopy. ^{1}H NMR spectra were recorded at room temperature (~25 °C) using a Bruker 400 MHz NMR spectrometer (see **Figure S1**). X-ray fluorescence spectrometry (Rigaku NEX DE, high-performance direct excitation EDXRF spectrometer) was used to examine elemental impurities. Analyses were performed directly on sample surfaces under low-, mid-, and high-energy excitation conditions to improve sensitivity across a broad range of elements. The XRF results are summarized in **Table S1** and confirm

the presence of trace elements in waste expanded polystyrene (EPS), particularly Br, Fe, Ti, Cr, and Zn at very low mass fractions (wt%), consistent with literature and typically associated with styrene production catalysts, polymer additives and residual processing contaminants.

Synthesis of multichannel carbon nanofibers

Multichannel carbon nanofibers were fabricated by using an electrospinning technique. The precursor solution contained 10 wt% polyacrylonitrile and 20 wt% of expanded polystyrene in 10 mL of N,N-dimethylformamide (DMF) in an equal ratio. The solution was then electrospun at a voltage of 20 kV with a working distance of 18 cm between the needle and the rotating drum collector, which was covered with aluminum foil. The flow rate of the precursor solution from the syringe was kept at 0.5 mL h^{-1}. The solution was spun for 5 h. Then the obtained polyacrylonitrile/expanded polystyrene nanofibers were calcined in the air at 250 °C for 2 h using a heating rate of 2 °C min^{-1} in a muffle furnace. This step stabilized the PAN (polyacrylonitrile) nanofiber by partial cyclization and oxidation [1] to prevent the fiber melting or deforming during subsequent higher-temperature carbonization in a tube furnace at 800 °C for 1 h under a nitrogen atmosphere using a heating rate of 5 °C min^{-1}.

Synthesis of Hollow $NiFe_2O_4$ nanofibers

Hollow nickel ferrite nanofibers were synthesized directly on multichannel carbon nanofibers by a one-step hydrothermal synthesis accompanied by a low-temperature calcination. In the synthesis, 30 mL of deionized water, 5 mL of anhydrous ethanol, 4 mmol of $FeCl_2.6H_2O$, and 16 mmol of urea ($CO(NH_2)_2$) were mixed step-by-step under continuous stirring at room temperature (~25 °C). After that, 2 mmol of $NiCl_2 \cdot 6H_2O$ and 21 mmol of NH_4F were added into the mixture. A distinct colour change of the resultant mixture was observed from light orange to the bluish-green. The resultant mixture was constantly stirred for 20 min. Then 80 mg of activated multichannel carbon nanofibers were put into the solution and stirred for 30 min to ensure that the resulting fiber mat was in full contact with the solution, and then the as-obtained mixture was poured into a 50 mL polytetrafluoroethylene (Teflon)-lined stainless steel autoclave. The autoclave was placed in an electric oven at 120 °C for 12 h. After this time, the reaction mixture was allowed to cool naturally to room temperature in the air. Once cool, the

material was taken out and washed repeatedly with ethanol and deionized water. Finally, the cleaned nickel ferrite decorated multichannel carbon nanofibers were placed in an oven and dried at 60 °C for 12 h. Finally, they were heated to 350 °C for 2 h in an air atmosphere, during which the carbon was converted to carbon dioxide, and hollow nickel ferrite nanofibers were obtained.

Synthesis of pristine $NiFe_2O_4$

The same hydrothermal method was used for the synthesis of pristine nickel ferrite ($NiFe_2O_4$). All the reagents, quantities, and reaction conditions were kept the same, except that the activated multichannel carbon nanofibers were not added into the autoclave. The obtained nickel ferrite was washed repeatedly with ethanol and deionized water, and then it was placed in an oven and dried at 60 °C for 12 h. Like the previous procedure, the material was calcined at 350 °C for 2 h in a muffle furnace in the air to obtain the nickel ferrite ($NiFe_2O_4$) particles.

Electrocatalyst characterization

The functionalization of the multichannel carbon nanofibers was confirmed using Fourier transform infrared spectrometry (FTIR, Jasco FR/IR 4100) with a resolution of 0.7 cm^{-1}. The surface morphologies, structures, and elemental mapping were studied by ultra-high resolution scanning electron microscopy (UHR-SEM, TESCAN CLARA) equipped with Energy X-ray Dispersive Spectrometry (EDX, Oxford Instruments UltimMax 65). The specific surface area and pore size distributions were obtained via the Brunauer-Emmett-Teller (BET) method by a physisorption analyzer (Anton Paar Quadrasorb Evo and Autosorb iQ-MP). The crystal structures were studied by X-ray diffraction (Rigaku MiniFlex) using a Cu Kα X-ray source. The diffraction angle 2θ was scanned from 10° to 80° at a rate of 2° per minute. Data analysis was performed using Rigaku SmartLab Studio-II software (Rigaku Corporation, 2014). TEM images were taken using a FEI Tecnai G2 F30 instrument operating at 300 kV to observe the hollow channels within the fibers. TEM samples were prepared directly on carbon coated-copper grids (carbon film, 400 mesh Cu). The lateral distribution of elements and chemistry at the surface of the prepared catalyst was analyzed by X-ray photoelectron spectroscopy (XPS, Axis Supra, Kratos, UK). The X-ray source utilized monochromated Al Kα radiation (1486.6 eV, 30 mA). The C 1s peak of all samples was adjusted to 284.8 eV for normalization. All data

were fitted using ESCApe software, which employed Gaussian-Lorentzian fitting to analyze each component peak (C1s, N1s, O1s, Ni 2p, and Fe 2p).

Electrochemical measurements

Electrochemical measurements were performed with a Gamry 1100E electrochemical workstation. All the experiments were performed at room temperature with a conventional three electrode electrochemical cell set-up; Pt wire was used as the counter electrode, Hg/HgO (CH Instruments, Inc., USA) was used as the reference electrode, and the various catalyst materials deposited on nickel foam were used as working electrodes. The catalyst ink for adhering materials to the working electrode was prepared by finely grinding 5 mg of the sample and ultrasonically dispersing it in 190 μL of DMF and 10 μL of Nafion solution for 2 h. 20 μL of this slurry was drop casted onto an area of 0.5 cm^2 of nickel foam and dried in air, resulting in a mass loading of around 0.001 g cm^{-2}. The electrochemical measurements were carried out in freshly prepared 1.0 M aqueous potassium hydroxide (KOH) solution, made with distilled water. In all electrochemical measurements, the reference electrode was calibrated to the reversible hydrogen electrode (RHE) scale based on the equation $E_{RHE} = E_{(Hg/HgO)} + (0.059 \times pH) + 0.098$ V.[2] In this work, the pH was 13.85. Linear sweep voltammetry (LSV) with a scan rate of 5.0 mV s^{-1} was conducted without iR-compensation. Electrochemical impedance spectroscopy (EIS) measurements were performed in the frequency range from 10^5 to 0.1 Hz. The EIS data were fitted to an equivalent electrical circuit that yielded the smallest chi-squared (χ^2) value using Gamry Echem Analyst software. The effective electrochemical surface area of a catalyst is directly correlated to the electrochemical surface roughness factor (R_f). The R_f is linked with the double layer capacitance (C_{dl}) such that ESCA $\propto R_f \propto C_{dl}$.[3] The double layer capacitance C_{dl} was calculated by cyclic voltammetry measurements at various scan rates in the range 50 to 500 mV s^{-1}. Anodic (j_a) and cathodic (j_c) current densities were recorded and plotted at 0.516 V_{RHE}. The specific capacitance (C_s) of the substrate was taken as the benchmark, with a literature value for C_s of the smooth oxide surface of nickel foam being 0.04 mF cm^{-2} in the non-faradaic region.[4] The ratio C_{dl}/C_s value gives the electrochemically active surface area (ECSA).[5] Chronoamperometry was recorded for 80 h continuously at a constant potential of −0.083 V *vs* RHE without iR-compensation. After 80 h, linear sweep voltammetry was undertaken, and the performance was compared with linear sweep voltammograms obtained before chronoamperometry to evaluate the stability of the electrocatalysts.

Faradaic efficiency calculation

A 250 µL sample of the gas collected from the cathodic headspace of the H-cell was analyzed using gas chromatography. The measurements were performed on an Agilent 8860 gas chromatography system equipped with a thermal conductivity detector, incorporating two Porapak Q columns and a MoleSieve 13X column. Prior to analysis, the gas chromatography system underwent calibration using certified gas mixtures (1%, 2%, 3%, and 5% H_2 in Ar) sourced from CK Gas Products Limited, UK. Faradaic efficiency was calculated by dividing the amount of H_2 gas experimentally detected by the "theoretical amount" of H_2 gas, i.e. that which would have been produced if all the charge passed had been used to generate hydrogen. The formula used for calculating the number of moles of hydrogen that would be produced by a system operating at 100% faradaic efficiency (the "theoretical" value) is:[6]

$$Q / F Z = n \qquad \textbf{(S1)}$$

Where, **n** represents the number of moles of the product, **Q** represents the total charge passed in coulombs during the electrochemical process, **F** is the Faraday constant (96,485 C/mol), and **Z** specifies the number of electrons required to produce one molecule of the resultant product, which is 2 for the hydrogen evolution reaction.

Relative Energy Difference for Polyacrylonitrile and Waste Polystyrene foam with Dimethylformamide

The Hansen solubility parameter estimates the compatibility of a solute with a solvent. In the precursor solution for electrospinning, polyacrylonitrile and waste polystyrene are the solutes, while dimethylformamide serves as the solvent. The relative energy difference between the solvent and solute is determined using the Hansen solubility parameters alongside the interaction radius (R_o). The relationship is expressed as relative energy difference = R_a/R_o

$$R_a = \sqrt{4(\delta_{D2} - \delta_{D1})^2 + (\delta_{P2} - \delta_{P1})^2 + (\delta_{H2} - \delta_{H1})^2} \qquad \text{(S2)}$$

Here, δD represents the energy from dispersion forces, δP represents the energy from intermolecular forces, δH is the energy associated with hydrogen bonding, and δ is the Hildebrand or total cohesion parameter. The value of the relative energy difference points towards the following conclusions:

- relative energy difference > 1 indicates poor solubility of the solute in the solvent.
- relative energy difference = 1 suggests partial solubility.
- relative energy difference < 1 implies that the solute will dissolve readily in the solvent.

The Hildebrand solubility parameter, which predates the Hansen parameters, is useful in determining the degree of solubility between substances, especially polymers. Differences in cohesive energy density (δ) between materials can predict their solubility: the smaller the difference, the better the miscibility.

Crystallite size: The crystallite size of the material was determined using the Scherrer equation:[7]

$$D = \frac{k\lambda}{\beta cos\theta} \qquad \text{(S3)}$$

D is crystallite size in the sample, K is the shape factor (0.89 in case of nanoplatelets), **λ** is the wavelength of X-ray source (Cu Kα. λ=1.54Å) and β is the full width at half maximum (FWHM) of the diffraction peak in radians. The FWHM was calculated by fitting the XRD peaks using a Lorentzian function. θ is the Bragg angle.

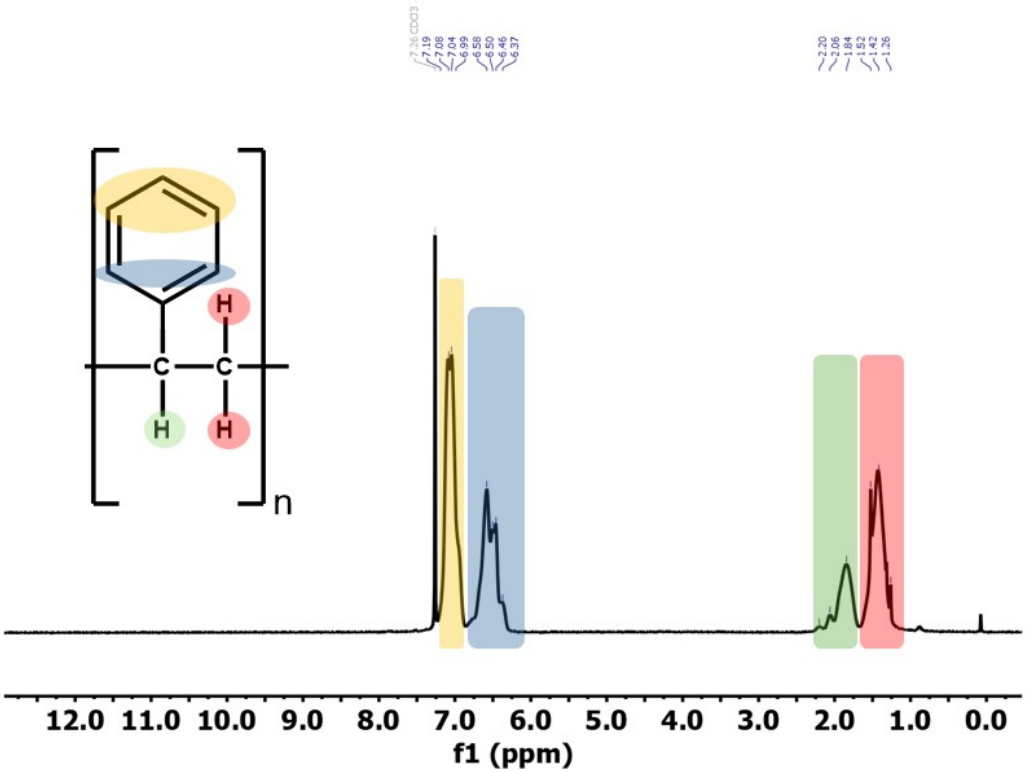

Figure S1: ^{1}H NMR of the waste expanded polystyrene starting material.[8-9]

Table S1. XRF analysis of waste expanded polystyrene showing elemental concentrations (in g/cm^2)**.**

Element	Average mass%
Na	0.051
Si	0.001
P	0.003
S	0.096
Cl	0.096
K	0.058
Ca	0.016
Ti	0.039
V	0.007
Cr	1.844
Mn	0.305
Fe	0.003
Ni	0.001
Cu	0.001
Zn	0.001
As	0.001
Br	0.002
Rb	0.009

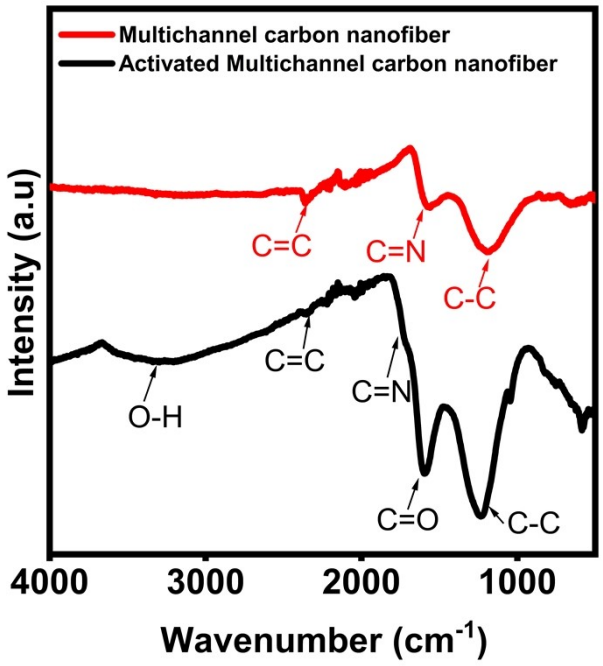

Figure S2: FTIR spectra showing the functionalisation of the surface of the multichannel carbon nanofibers after activation with $KMnO_4$.

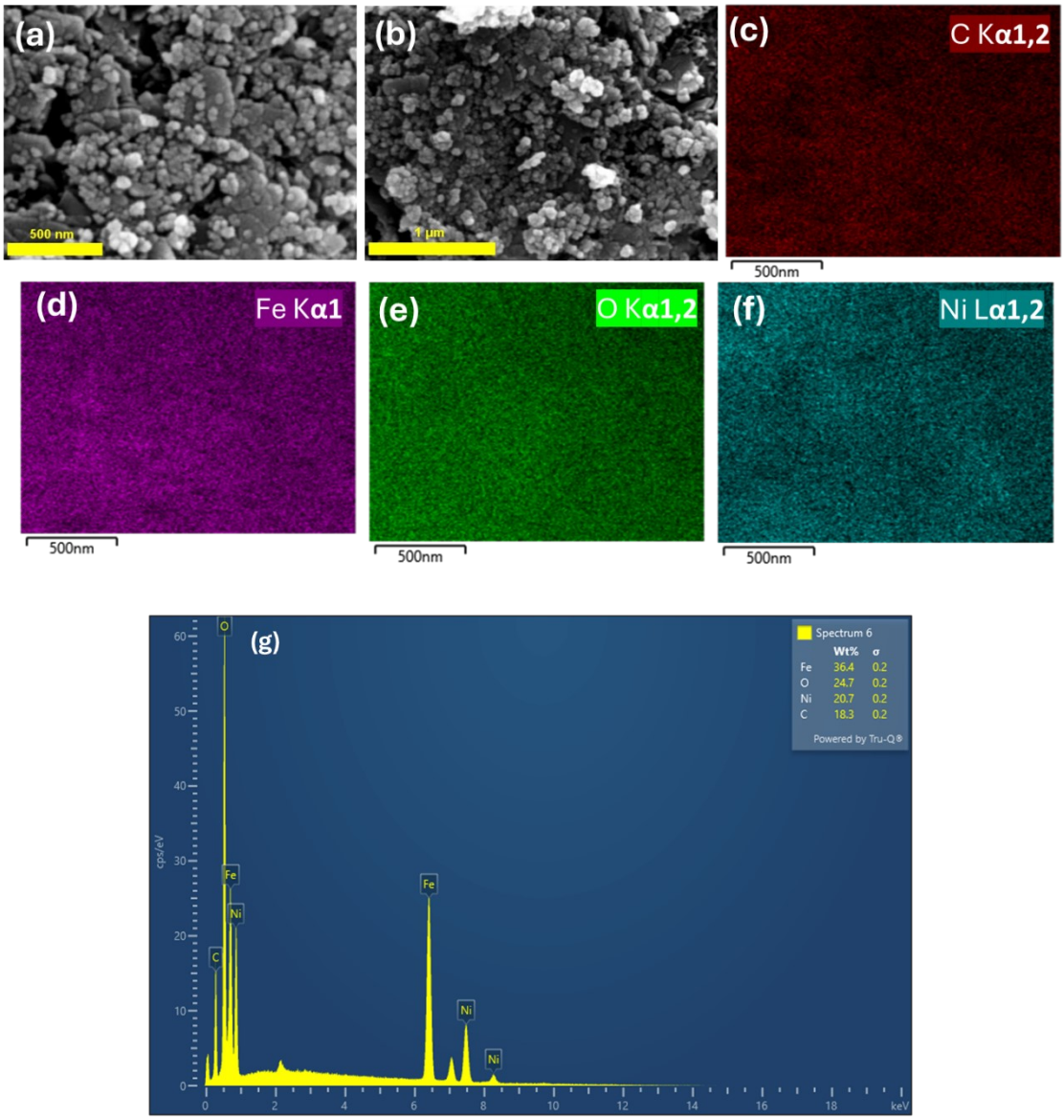

Figure S3: (a-b) SEM images of pristine $NiFe_2O_4$ at various magnifications; **(c-f)** Elemental maps of C, Fe, O and Ni present in the sample; **(g)** EDX spectrum of pristine $NiFe_2O_4$.

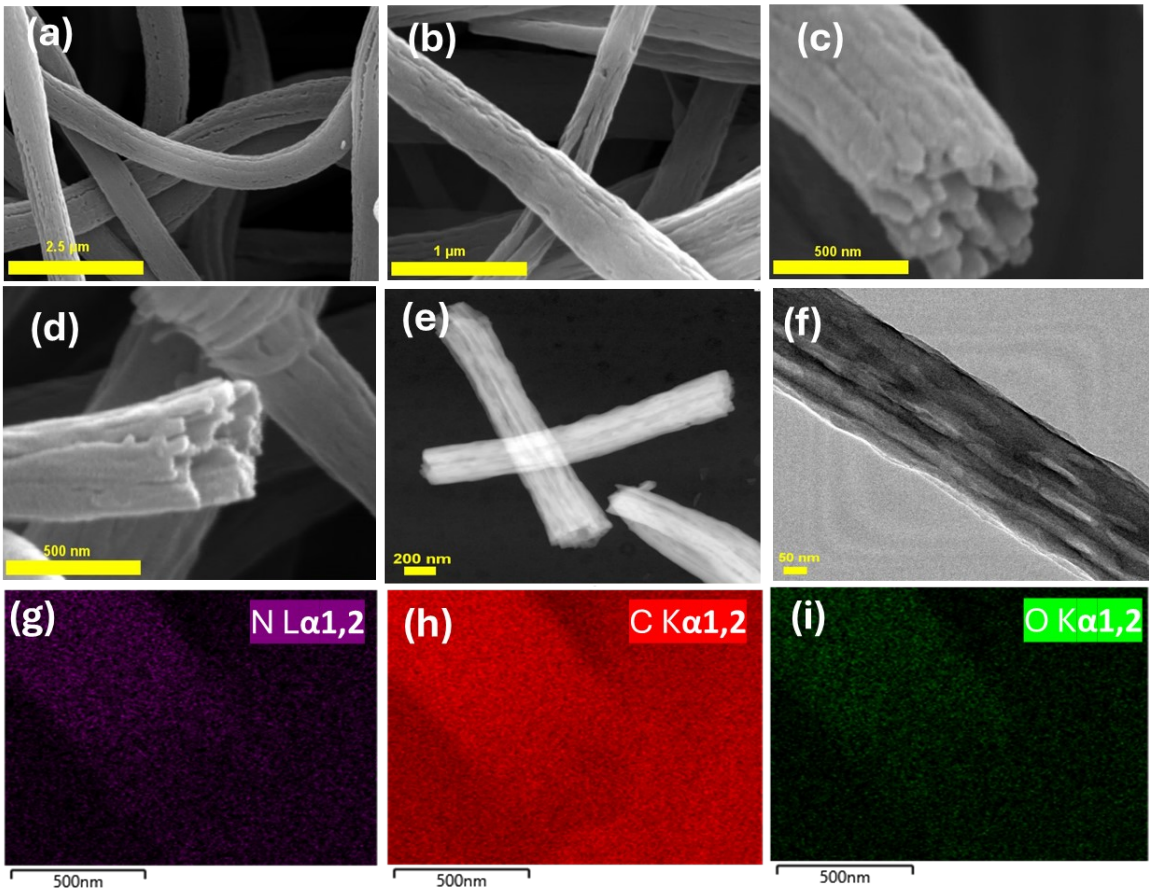

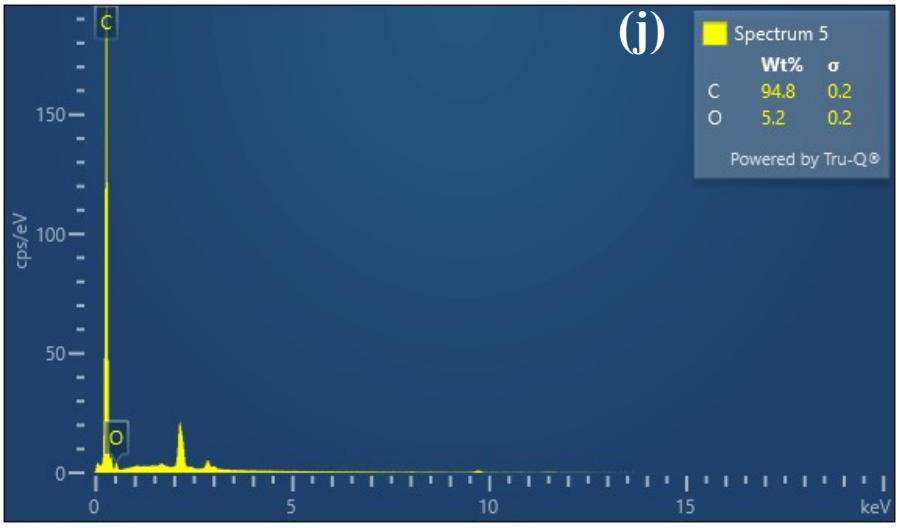

Figure S4: (a-d) SEM images of multichannel carbon nanofibers at various magnifications; **(e-f)** TEM images; **(g-i)** Elemental maps of N, C and O present in the sample; **(h)** EDX spectrum of sample.

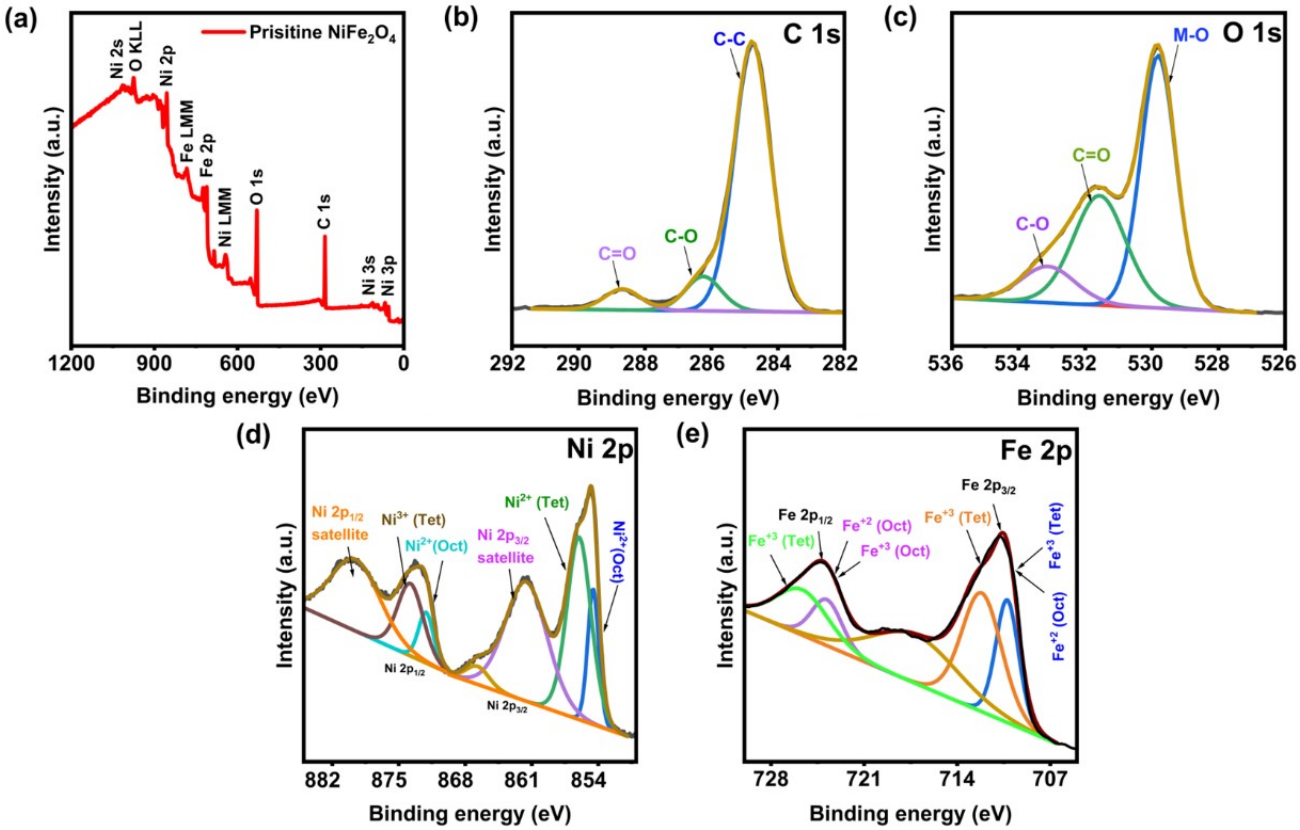

Figure S5: Full scan **(a)** and high-resolution XPS spectra of pristine $NiFe_2O_4$; (**b**) C 1s; **(c)** O 1s; **(d)** Ni 2p; and **(e)** Fe 2p.

Table S2: Quantitative analysis of the XPS data of hollow and pristine $NiFe_2O_4$ samples

Elements	Sub fittings	Hollow porous $NiFe_2O_4$ nanofiber		Pristine $NiFe_2O_4$	
		B.E (eV)	Area (%)	B.E (eV)	Area (%)
Ni 2p1/2	Ni^{3+} (tet)	873.57	10.88	873.77	10.69
	Ni^{2+} (oct)	871.92	3.97	872.12	4.37
Ni 2p3/2	Ni^{3+} (tet)	855.98	24.67	856.02	25.23
	Ni^{2+} (oct)	854.40	8.90	854.54	8.51
Fe 2p1/2	Fe^{3+} (tet)	725.31	14.92	725.67	15.34
	Fe^{2+} (oct)	723.56	9.23	723.81	9.06
Fe 2p3/2	Fe^{3+} (tet)	711.92	31.08	712.16	30.68
	Fe^{2+} (oc/tet)	710.13	18.86	710.24	18.13

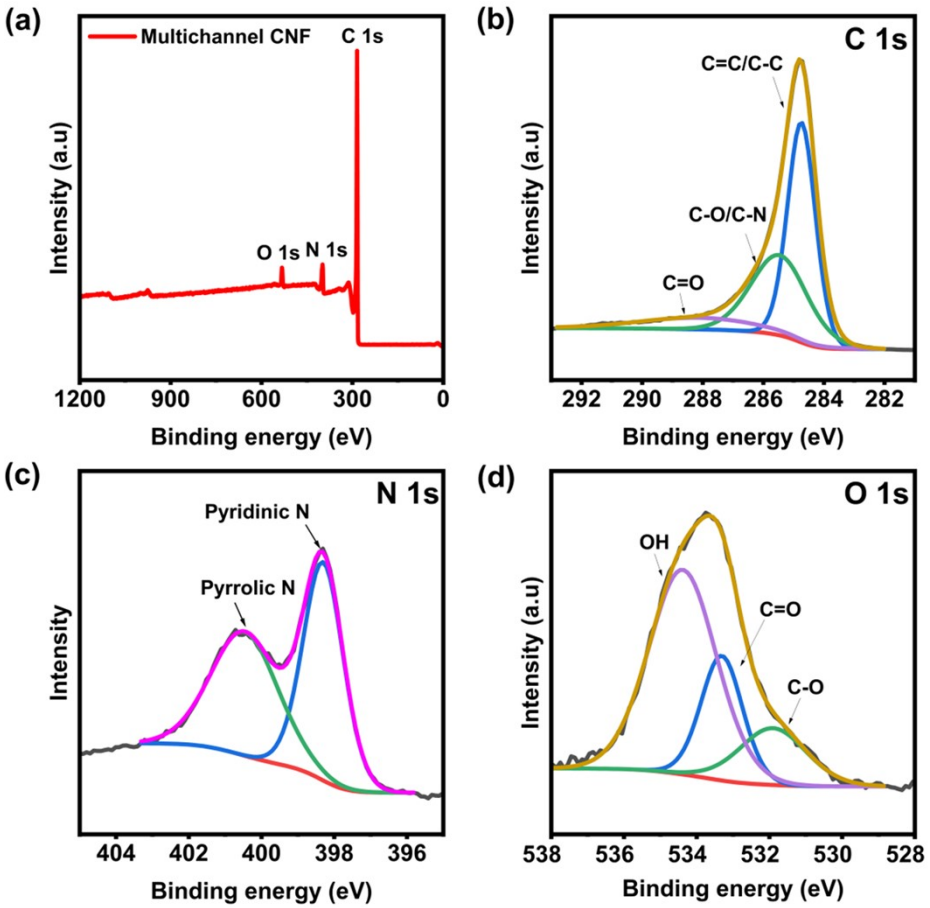

Figure S6: Full scan **(a)** and high-resolution XPS spectra of the multichannel carbon nanofibers; **(b)** C 1s; **(c)** N 1s; **(d)** O 1s.

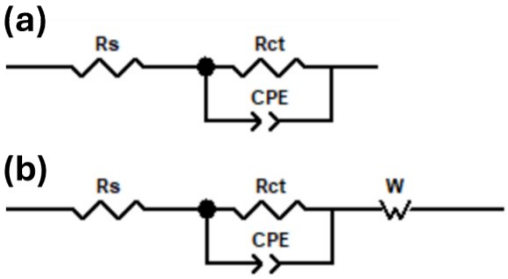

Figure S7: The equivalent circuit model fitting for the EIS Nyquist plots: (a) constant phase element model and (b) constant phase element diffusion model with Warburg impedance component.

Table S3 Each component of the proposed equivalent circuits for the EIS of the various materials.

Sample	Charge transfer resistance (R_{ct}) ohm cm^2	Solution Resistance (R_s) ohm cm^2	Constant Phase element (Y_o)	Alpha (n)	Infinite Warburg (W)	chi squared (χ^2)	Electrical circuit model (Fig S7)
Hollow $NiFe_2O_4$ nanofibers	42.42	3.50	958.3×10^{-6}	0.75	95.19×10^{-3}	2.34×10^{-3}	b
Pristine Nickel ferrite	293.01	2.78	537.3×10^{-6}	0.77	-	1.31×10^{-3}	a
Multichannel carbon nanofibers	73.39	3.91	648.2×10^{-6}	0.76	73.4×10^{-3}	3.43×10^{-3}	b
Nickel Foam	431.42	5.17	320.1×10^{-6}	0.85	-	5.7×10^{-3}	a

The rate of charge transfer at the electrode–electrolyte interface for hollow nickel ferrite nanofibers and pristine nickel ferrite was evaluated from the exchange current density (j_o) using the equation below:

$$j_o = RT/nF\ \theta \qquad \textbf{(S4)}$$

where R is the universal gas constant (8.314 J mol^{-1} K^{-1}), T is the reaction temperature (293 K), n is the number of electrons transferred ($2e^-$ for HER), F is the Faraday constant (96485 C mol^{-1}), and θ is the charge transfer resistance for each catalyst obtained from fitting an equivalent circuit to the EIS data given in Table S3.

For hollow $NiFe_2O_4$ nanofibers, θ = 42.42 Ω

$$j_o = 8.314 * 293 / 2 * 96485 * 42.46$$

$$= 301\ \mu A\ cm^{-2}$$

For pristine nickel ferrite, θ = 293.01 Ω

$$j_o = 8.314 * 293 / 2 * 96485 * 293.01$$

$$= 43\ \mu A\ cm^{-2}$$

The hollow nickel ferrite nanofiber catalyst revealed a higher j_o (301 μA cm^{-2}) than that of pristine nickel ferrite (43 μA cm^{-2}), demonstrating a higher electron transfer rate for hydrogen production.

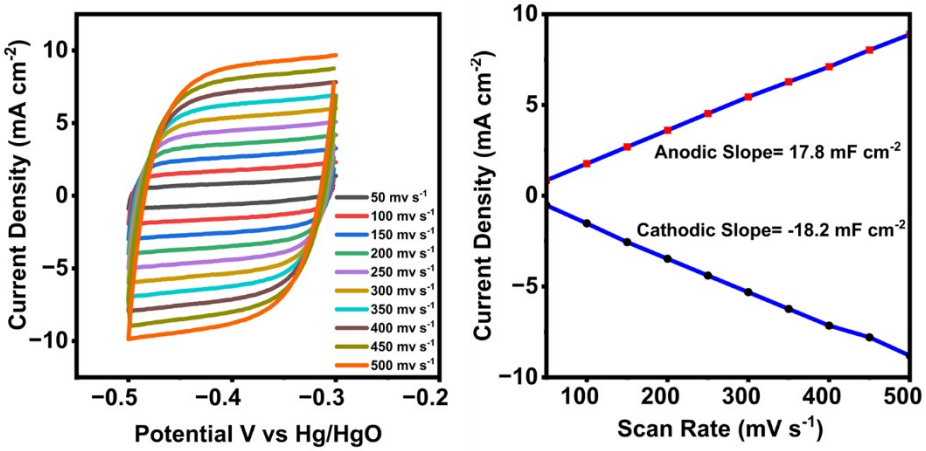

Figure S8: Cyclic voltammetry of the hollow nickel ferrite nanofibers taken in the non-faradic region at different scan rates ranging from 50 to 500 mV s^{-1}.

The cyclic voltammetry data were recorded from −0.3 to −0.5 V vs Hg/HgO at different scan rates ranging from 500 to 50 mV s^{-1}, as shown in above figure. The current densities at −0.4 V vs Hg/HgO were taken for each cycle and plotted against the corresponding scan rate. Then, the double layer capacitance (Cdl) was determined from the slope of the linear fit of the current density vs the scan rate.[4]

Electrochemical surface area (ECSA) was calculated using formula

$$ECSA = \frac{C_{dl}}{C_s} \qquad \textbf{(S5)}$$

Where C_{dl} is the double-layer capacitance, and C_s is the specific capacitance. For nickel foam, the C_s value is 0.04 mF cm^{-2} in basic conditions as reported in the literature.[10-11] From Figure S8, the hollow $NiFe_2O_4$ nanofibers have C_{dl} = 18 mF cm^{-2} and their ECSA relative to nickel foam is given by:

$$ECSA = \frac{18}{0.04} = 450\ cm^2/cm^2{}_{geometric}$$

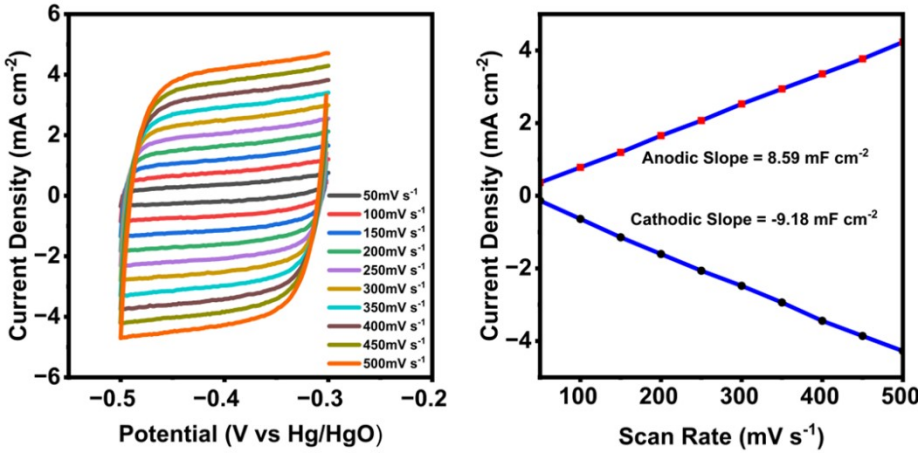

Figure S9: Cyclic voltammetry of the multichannel carbon nanofibers taken in the non-faradic region at different scan rates ranging from 50 to 500 mV s^{-1}.

ECSA for multichannel carbon nanofibers with C_{dl} = 8.88 mF cm^{-2} relative to nickel foam:

$$ECSA = \frac{8.88}{0.04} = 222 \ \ cm^2 \ / cm^2 \ _{geometric}$$

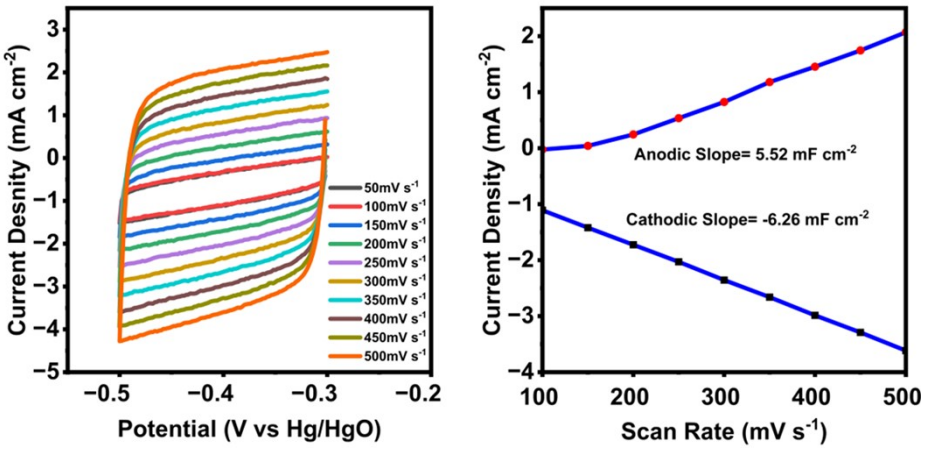

Figure S10: Cyclic voltammetry of the pristine nickel ferrite taken in the non-faradic region at different scan rates ranging from 50 to 500 mV s^{-1}.

ECSA for pristine nickel ferrite with C_{dl} = 5.89 mF cm^{-2} relative to nickel foam:

$$ECSA = \frac{5.89}{0.04} = \ 147 \ cm^2 \ / cm^2 \ _{geometric}$$

The polarization curves were normalized to the ECSA according to the following equation:

$$j_{ECSA}\,(mA/cm^2) = \frac{i \times 1000}{ECSA} \qquad \text{(S7)}$$

where i (A) is the current without any iR-drop, and ECSA is the electrochemical active surface area (cm^2) of the material. LSV polarization curves obtained after normalizing to the ECSA, shown below, demonstrate that hollow nickel ferrite nanofiber possesses higher intrinsic activity than pristine nickel ferrite.

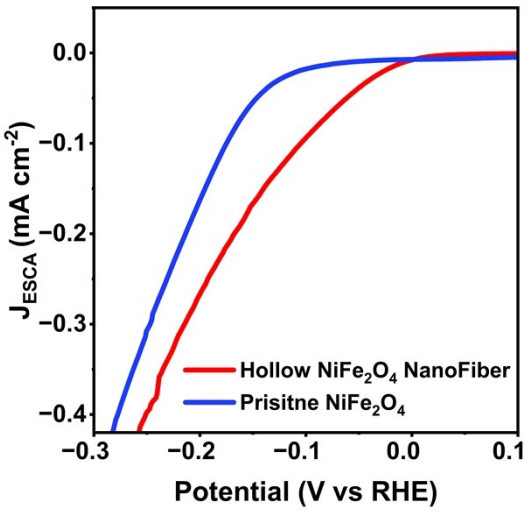

Figure S11: LSV polarization curves normalized to the ECSA.

For the normalization of the polarization curves to the BET surface area, the following equation was used

$$j_{BET}\,(mA/cm^2) = \frac{i \times 1000}{S \times BET\ surface\ area \times m_{loading}} \quad \text{(S8)}$$

where i (A) is the current without any iR-drop, S is the geometric area of nickel foam used (0.5 cm^2), BET_{area} is calculated from the nitrogen absorption-desorption isotherms, and $m_{loading}$ is the loading of catalyst on nickel foam (0.001 g cm^{-2}).

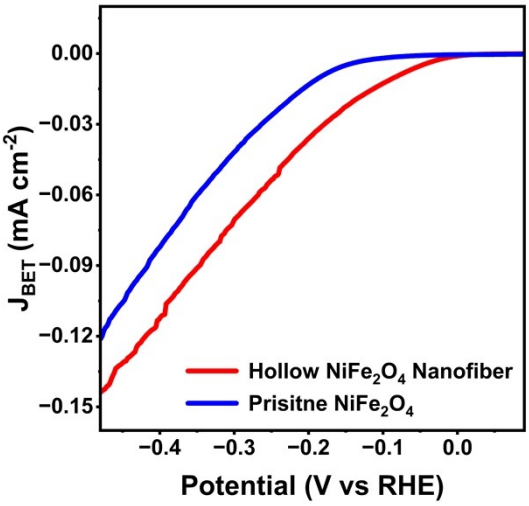

Figure S12: LSV polarization curves normalized to the BET surface area.

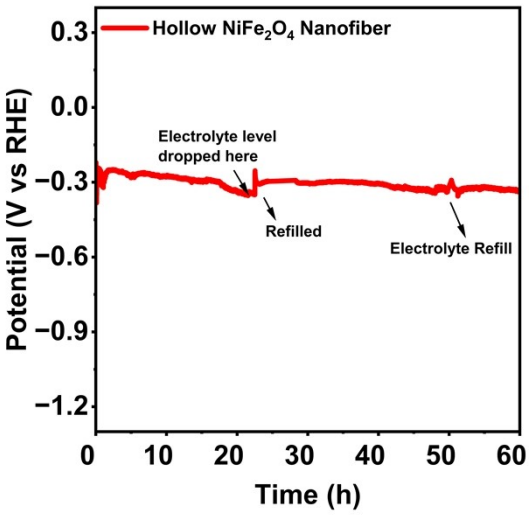

Figure S13: Chronopotentiometric stability test of hollow porous $NiFe_2O_4$ nanofibers at a current density of 100 mA cm^{-2} for 60 h.

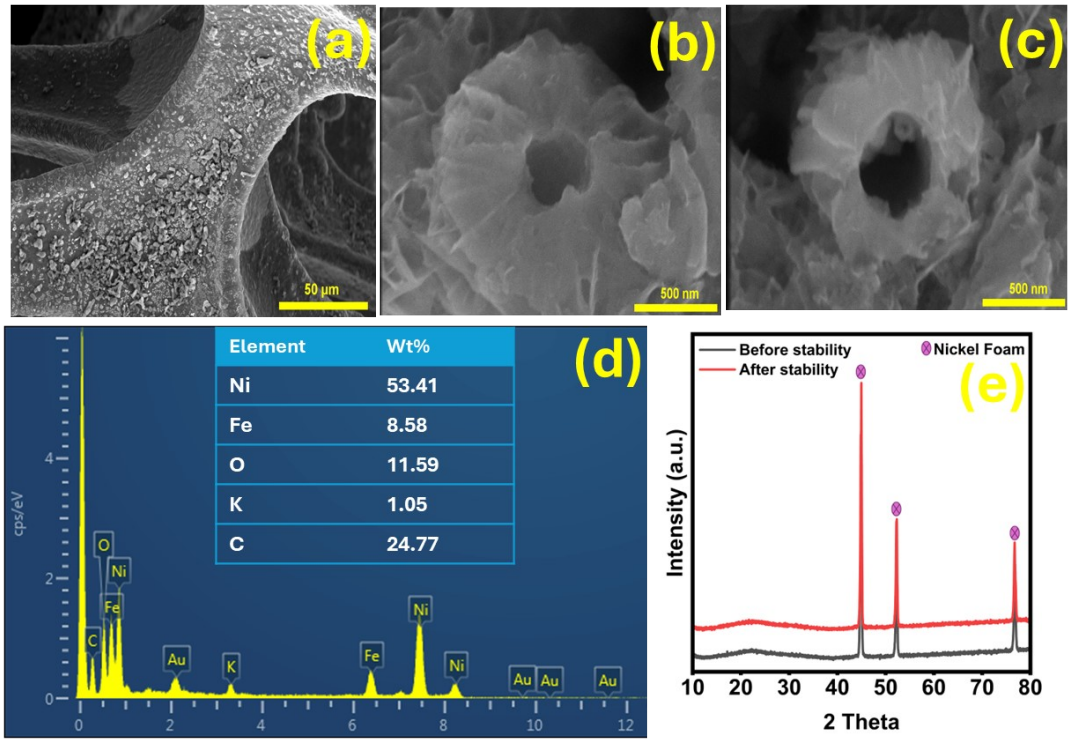

Figure S14: Post-electrolysis (60 h at 100 mA cm^{-2}) characterization of hollow porous $NiFe_2O_4$ nanofibers by (a-c) SEM; (d) EDX; (e) XRD.

The TOF was calculated at an overpotential of 100 mV using the following formula:

$$TOF = i \times NA / A \times F \times n \times \Gamma \qquad \textbf{(S6)}$$

Where i = current in Amps (0.061 A); NA= Avogadro's number (6.02×10^{23}), A = Geometrical surface area of the electrode (0.5 cm^2); F = Faraday's constant (96485 C mol^{-1}); n = number of electrons transferring (2 for HER); Γ = Surface concentration of atoms.

The surface concentration of atom/active sites was determined by running cyclic voltammetry (CV) for the hollow porous $NiFe_2O_4$ nanofibers at scan rate of 5 mA s^{-1} using the same three electrode system in 1 M KOH solution, and the area under the curve for the M^{3+} / M^{2+} redox couple was determined as shown in the figure below:

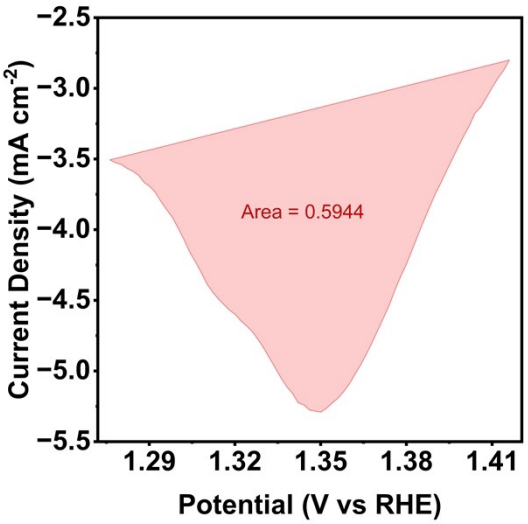

Figure S15: The area under the curve of the reduction peak of the M^{3+} / M^{2+} redox couple in the hollow nickel ferrite nanofiber material.

The area under the curve of the M^{3+} / M^{2+} redox couple = 0.000594 V A

Hence, charge is = 0.000594 V A / 0.005 V s^{-1} = 0.118 C

Then, number of electrons = 0.118 C/1.602 $\times 10^{-19}$ C = 7.36×10^{17} electrons

Hence, Γ = surface concentration of atoms = 7.36×10^{17} atoms

TOF at η = 200 mV

= i × NA / A × F × n × Γ

= $[(0.061A \times 6.022 \times 10^{23})] / [(0.5) \times (96485) \times (2) \times (7.36 \times 10^{17})$

= 0.516 ms^{-1}

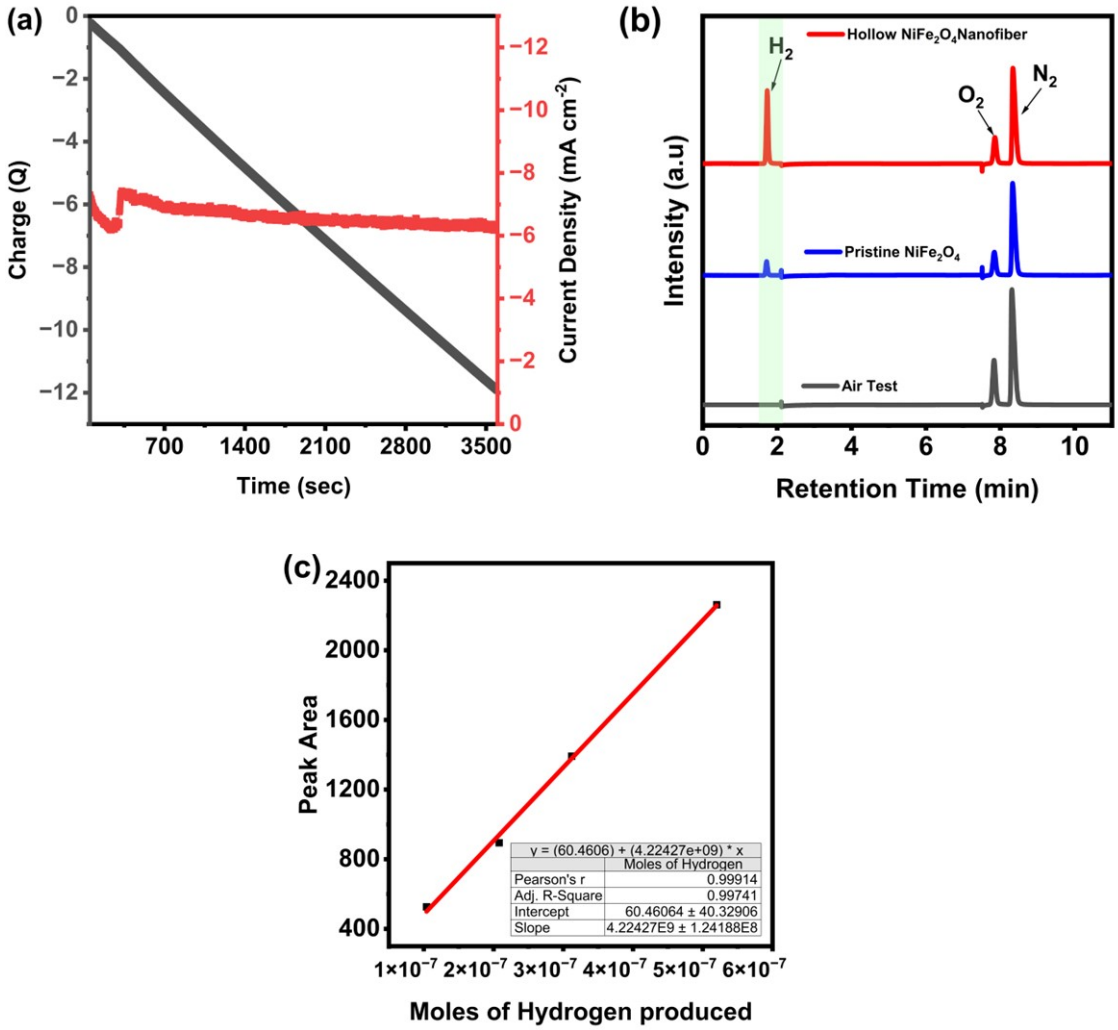

Figure S16: (a) Controlled potentiometry at a potential of −0.083V vs RHE for 1 h in an H-cell, (**b**) GC spectra obtained after controlled potentiometry at a potential of −0.083V vs RHE for 1 h in an H-cell for the hollow nickel ferrite nanofibers and pristine nickel ferrite, (**c**) calibration curve for hydrogen production.

References

1. Hameed, N.; Sharp, J.; Nunna, S.; Creighton, C.; Magniez, K.; Jyotishkumar, P.; Salim, N. V.; Fox, B., Structural Transformation of Polyacrylonitrile Fibers During Stabilization and Low Temperature Carbonization. *Polymer Degradation and Stability* **2016**, *128*, 39-45.
2. Wu, Y.; Liu, C.; Wang, C.; Yu, Y.; Shi, Y.; Zhang, B., Converting Copper Sulfide to Copper with Surface Sulfur for Electrocatalytic Alkyne Semi-Hydrogenation with Water. *Nature communications* **2021**, *12*, 3881.
3. Yin, X.; Sun, G.; Wang, L.; Bai, L.; Su, L.; Wang, Y.; Du, Q.; Shao, G., 3d Hierarchical Network Nico2s4 Nanoflakes Grown on Ni Foam as Efficient Bifunctional Electrocatalysts for Both Hydrogen and Oxygen Evolution Reaction in Alkaline Solution. *International Journal of Hydrogen Energy* **2017**, *42*, 25267-25276.
4. Martínez-Hincapié, R.; Wegner, J.; Anwar, M. U.; Raza-Khan, A.; Franzka, S.; Kleszczynski, S.; Čolić, V., The Determination of the Electrochemically Active Surface Area and Its Effects on the Electrocatalytic Properties of Structured Nickel Electrodes Produced by Additive Manufacturing. *Electrochimica Acta* **2024**, *476*, 143663.
5. Aziz, I.; Chen, X.; Hu, X.; Zhang, W. A.; Awan, R. J.; Rauf, A.; Arshad, S. N., Growth of Carbon Nanotubes over Carbon Nanofibers Catalyzed by Bimetallic Alloy Nanoparticles as a Bifunctional Electrode for Zn–Air Batteries. *RSC advances* **2023**, *13*, 11591-11599.
6. Li, Y.; Chen, J.; Cai, P.; Wen, Z., An Electrochemically Neutralized Energy-Assisted Low-Cost Acid-Alkaline Electrolyzer for Energy-Saving Electrolysis Hydrogen Generation. *Journal of Materials Chemistry A* **2018**, *6*, 4948-4954.
7. Hassanzadeh-Tabrizi, S., Precise Calculation of Crystallite Size of Nanomaterials: A Review. *Journal of Alloys and Compounds* **2023**, 171914.
8. Weill, G.; Vogl, O., Head-to-Head Polymers X: High Resolution Nmr Spectroscopy of Polystyrene and Poly (Vinyl Cyclohexane). *Polymer Bulletin* **1978**, *1*, 181-189.
9. Wackerly, J. W.; Dunne, J. F., Synthesis of Polystyrene and Molecular Weight Determination by 1h Nmr End-Group Analysis. *Journal of Chemical Education* **2017**, *94*, 1790-1793.
10. Son, Y. J.; Kawashima, K.; Wygant, B. R.; Lam, C. H.; Burrow, J. N.; Celio, H.; Dolocan, A.; Ekerdt, J. G.; Mullins, C. B., Anodized Nickel Foam for Oxygen Evolution Reaction in Fe-Free and Unpurified Alkaline Electrolytes at High Current Densities. *ACS nano* **2021**, *15*, 3468-3480.
11. Arshad, F.; ul Haq, T.; Khan, A.; Haik, Y.; Hussain, I.; Sher, F., Multifunctional Porous Nico Bimetallic Foams toward Water Splitting and Methanol Oxidation-Assisted Hydrogen Production. *Energy Conversion and Management* **2022**, *254*, 115262.